A Numerical Simulation and an Experimental Study on the Steady-State Levitation Characteristics of a Magnetic Ball Driven by External Electromagnets in a Fluid Tube: Applications to Micromachines in Human Blood Vessels

Zhanxiang Cui[1] – Yonghua Lu[1] ✉ – Yun Zhu[2] – Zezheng Wang[1] – Ziyuan Wang[1]

1 Nanjing University of Aeronautics and Astronautics, College of Mechanical and Electrical Engineering, China
2 Aero Engine Corporation of China, China
✉ nuaa_lyh@nuaa.edu.cn

Abstract *Research on micro-robots in the field of medicine has introduced innovative methods for treating various diseases. This study aims to expand the application of controllable micromechanical diagnoses and treatment within human blood vessels by designing a magnetic levitation ball system in a fluid-filled circular tube. The system enables a magnetic ball to be stably suspended along a specific path under the influence of an external magnetic field. Simulations of the system's electromagnetic field, flow field characteristics, and mechanical state were conducted by using finite element software. The study analyzed the effects of the ball's position, magnetic pole direction, driving current, and fluid flow rate on the forces acting on the magnetic ball. Joint simulations of the flow and magnetic fields were performed using the ANSYS Workbench platform, and a multi-objective optimization method was employed to determine the parameters for stable suspension. Experimental validation demonstrated the stable suspension of the magnetic ball in a fluid tube under an external magnetic field. The experiments revealed the relationships among the driving current, fluid flow rate, and the ball's stable suspension position, confirming the effectiveness of the simulation method and the feasibility of controlling object positions within fluid tubes.*

Keywords *magnetic levitation, blood vessel, steady-state levitation, biomedical micromachines, multi-objective optimization*

Highlights

- *Proposed a magnetic drive control for micro-devices in fluid tubes, aiding vascular disease treatment.*
- *Identified factors affecting a magnetic ball's steady position in blood vessels via simulations and tests.*
- *Developed a simulation model and an optimization method for better control of the magnetic ball.*

1 INTRODUCTION

In the medical field, interventional detection and procedures are essential for treating certain diseases, particularly cardiovascular blockages. Addressing the detrimental effects of cardiovascular disease is a significant concern within the global medical community. The integration of minimally invasive surgery and vascular robotics in patient treatment has increasingly become a mainstream research trend, showcasing considerable potential for practical application [1, 2]. In the traditional diagnosis and treatment of canaliculopathies, physicians often employ a guidewire mechanism to deliver microdevices to a targeted site. However, this method has several drawbacks, including limited controllability, inapplicability in narrow spaces, and a high risk of damaging the mucosa. Diagnostic and therapeutic devices based on micro-electro-mechanical systems (MEMS) represent a significant advancement for medical devices. Numerous innovations have been achieved in areas such as wireless endoscopes, micro-drug delivery systems, minimally invasive surgery, and in vivo detection. The application of these microdevices enables clinicians to conduct the diagnosis and treatment in a minimally invasive or non-invasive manner [3].

Researchers are exploring techniques for driving micromechanical devices within human body cavities. In biological tissues, micromachines are frequently powered by external magnetic fields, electric fields, light energy, chemical energy, and bioenergy [4]. For instance, Cai et al. employed Helmholtz coils to generate external magnetic fields to drive microrobots through mucus tubes [1]. Similarly, Li et al. utilized an external magnetic field and bacteria to drive robots in blood vessels [5]. Fu et al. developed magnetically-driven microrobots powered by an oscillating tail [6].

The actuation of micro-robots using external magnetic fields is less harmful and more controllable within the human lumen [7]. Helmholtz and Maxwell coils are commonly used to generate external magnetic fields [8-10]. However, the coils need to completely encircle the target space, resulting in a very limited controllable range for the micro-robot. Hamal Marino et al. proposed an active magnetic levitation method to achieve controlled spiral motion of a micro-robot in viscous liquids [11]. Chi et al. invented a low-torque micro-robot designed for controllable motion within the human esophagus [12]. Furthermore, Li et al. developed a two-dimensional actuation technique for magnetic particles in confined spaces [13]. The magnetic levitation control technique enables precise motion control of micro-objects in small spaces [14, 15]. Due to the biologically harmless nature of magnetic fields, magnetic levitation can also be applied in the field of medicine for detection, analysis, and cell assembly [16].

Controllable micro-robots in human body cavities are usually equipped with helical structures [17], oscillating components [18],

DOI: 10.5545/sv-jme.2024.1080

and permanent magnets [19], powered by reactive forces with liquids. However, their traveling speed is slow, and they easily collide with the lumen wall, causing damage to body tissue. There is little research on the precise position control of micro-machines within the complex environment of human blood vessels. Numerical simulations are also commonly employed to study the motion characteristics of micro-robots within pipelines. For instance, Derbal et al. [20] investigated the effect of flow field parameters on the flow characteristics of magnetic fluids with nanoparticles. Meanwhile, Gkountas et al. [21] conducted simulations to analyze the impact of rotating magnetic field parameters on the forces and displacements of micro-robots in fluids, which has been applied to the structural design of micro-mechanics.

This paper presents a study on the development of external magnetic drive technology for micromachines operating within human blood vessels. In this system, permanent magnets serve as target objects, while a gradient magnetic field acts as the driving source, enabling the manipulation of controlled objects from a distance without physical contact. Specifically, a one-dimensional magnetic levitation ball system was designed and implemented within a fluid tube to investigate the effects of flow field and magnetic field parameters on the position control of suspended objects, as well as the influence of physical field characteristics. The Maxwell and Fluent finite element simulation platforms were utilized to perform numerical calculations on the distribution characteristics of the magnetic and flow fields, as well as the impact of physical parameters on the stress state of the suspended body. The workbench platform was employed to calculate the flow and magnetic fields of the suspended body, utilizing a multi-objective optimization method to determine the steady-state levitation parameters of the magnetic ball. Finally, a steady-state levitation experiment of the magnetically driven ball in a fluid tube was conducted and compared with the results from numerical simulations.

2 METHODS & MATERIALS

2.1 The Principle of a Magnetic Levitation Ball System Driven by an External Magnetic Field in a Fluid Tube

A magnetic levitation ball system is proposed to simulate the operational scenarios of micro-robotics within a fluid tube. The system, illustrated in Fig. 1, consists of a magnetic ball, a controller, a driving circuit module, a position measurement module, an electromagnetic driver, and a fluid tube. The magnetic ball is attracted by the magnetic force generated by the electromagnet. The controller manages the driving circuit to supply the appropriate current to the electromagnet, while the measurement circuit utilizes data from multiple position sensors to provide real-time position feedback of the magnetic ball to the controller. The magnetic ball can maintain a stable suspension state within the tube through the combined effects of blood flow and the attraction of the electromagnet.

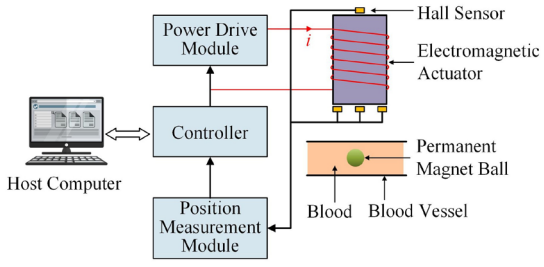

Fig. 1. Schematic diagram of the magnetic levitation ball system driven by an external magnetic field

As illustrated in Fig. 2, the structure of the electromagnet comprises a hollow cylindrical solenoid wound with multiple layers of enameled wire. The relevant parameters of the electromagnet are outlined in Table 1. Magnet design ensures that it can withstand high currents while providing sufficient suspension distance of the ball. The magnetic ball is a spherical permanent magnet made of NdFeB, with its adjacent hemispheres representing the north and south poles, respectively. The electromagnet can suspend magnetic balls with diameters ranging from 5 mm to 15 mm. Given the long-range position detection capabilities and minimal obstruction to the fluid, a magnetic ball with a diameter of 12.7 mm was selected. The mass of the ball m is 8.15 g, and the surface magnetic induction intensity B_s is 677.3 mT. The suspension distance range of the magnetic ball in air is [-15 mm, -38 mm] (from the lower end face of the electromagnet coil to the center of the magnetic ball). Fig. 3 shows a photo of the magnetic ball at the farthest suspension position.

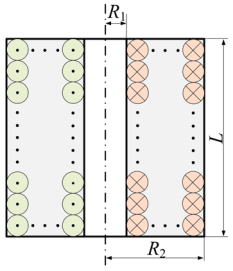

Fig. 2. Schematic diagram of the structure of the electromagnet

Table 1. Related parameters of electromagnet

Parameters	Symbol	Value
Number of coil turns	N	1489
Inner radius	R_1	8 mm
Outer radius	R_2	31.5 mm
Height	L	65 mm
Resistance	R_c	0.5 Ω

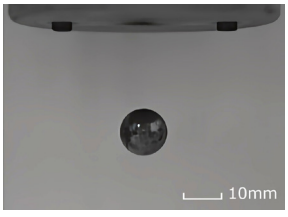

Fig. 3. The farthest suspension position of the magnetic ball in the air

2.2 Modeling

The electromagnetic and fluid resistance forces acting on a stably suspended ball in blood are challenging to establish through mathematical derivation. Therefore, the relationship between the electromagnetic field, fluid parameters, and the forces on the magnetic ball is determined using finite element simulation tools. By varying the driving current of the electromagnet, the electromagnetic force acting on the ball can be modified, resulting in different equilibrium states at various positions. Consequently, by controlling the driving current, the position of the magnetic ball within the blood vessel can be adjusted. A proportional–integral–derivative (PID) controller is used to achieve stable suspension of the magnetic ball. A Hall sensor is utilized to detect the position of the ball as feedback. Based on the difference between the current position and the target position, the controller adjusts the driving current of the electromagnet in real-time to maintain the ball's suspension at the desired position. When

the ball is adjusted and suspended in a fixed position, the driving current of the electromagnet remains constant, while the forces acting on the magnetic ball are balanced.

Fig. 4 illustrates the force analysis of the magnetic ball, where $\mathbf{F_m}$ represents the electromagnetic force, $\mathbf{F_d}$ denotes the fluid force, $\mathbf{G}$ signifies the gravitational force, and $\mathbf{F_u}$ indicates the buoyancy of the magnetic ball. $\mathbf{G}$ and $\mathbf{F_u}$ are always oriented vertically. With a constant blood flow rate, the magnetic ball can achieve the force balance at multiple positions. Fig. 4 depicts two positions of the magnetic ball: one near to the electromagnet and the other farther away. Assuming both positions are in a state of force balance, their force conditions and the required driving current will differ.

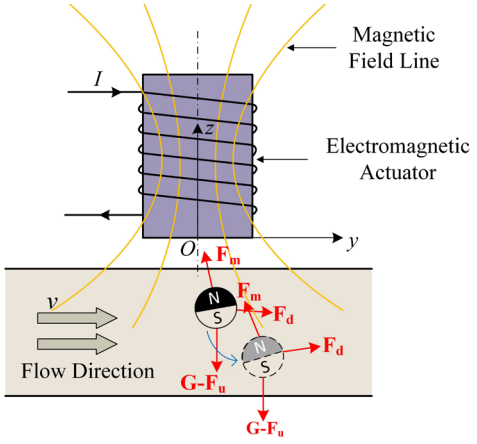

Fig. 4. Schematic diagram of the force analysis of the magnetic ball

Within blood vessels, the magnetic ball experiences fluid drag, buoyancy, and gravity. The electromagnet exerts an upward electromagnetic force on the ball. This force can be expressed as [22]:

$$\mathbf{F} = \mathbf{p}\nabla\mathbf{B} = \frac{3B_s}{2\mu_0}V_b\left(\frac{\partial\mathbf{B}}{\partial x}\mathbf{i} + \frac{\partial\mathbf{B}}{\partial z}\mathbf{k}\right), \tag{1}$$

where the magnetic dipole moment is denoted by $\mathbf{p}$, the magnetic permeability of air is denoted by μ_0, the surface magnetic induction of the magnetic ball is denoted by B_s, V_b represents the volume of the magnetic ball, $\mathbf{B}$ represents the magnetic flux density, $\mathbf{i}$ is a horizontal unit vector, and $\mathbf{k}$ is a vertical unit vector.

The upward buoyancy acting on the magnetic ball can be expressed as:

$$\mathbf{F_u} = \rho\mathbf{g}V_b. \tag{2}$$

In the bloodstream, a spherical object experiences two types of fluid resistance. One is the viscous resistance caused by friction, which can be expressed by Stokes' law as [23]:

$$f_1 = 6\pi\eta Rv. \tag{3}$$

The other is the pressure difference resistance, which can be expressed as [24]:

$$f^2 = \frac{1}{2}\zeta A\rho v^2, \tag{4}$$

where ρ represents the density of blood, $\mathbf{g}$ is gravitational acceleration, η is the viscosity of blood, R is the the radius of the magnetic ball, v is the relative velocity of the ball to the blood, ζ is the resistance coefficient, and A is the projected area of the ball perpendicular to the direction of blood flow.

In the following sections, finite element simulation software is employed to calculate the electromagnetic and fluid forces acting on the ball. The parameters of the electromagnetic field and the flow field are optimized to determine the conditions for force balance of the magnetic ball. Additionally, the appropriate drive current is selected for precise control of the target position.

2.3 Numerical Simulation Method of Electromagnetic Field

ANSYS Maxwell software is used to calculate the electromagnetic field by solving Maxwell's equations [25], as presented in Eq. (5). Three-dimensional modeling and simulation parameter settings are conducted. The electromagnetic model is shown in Fig. 5. The relative magnetic permeability of the magnetic ball is 1.1, and its coercive force is -808500 A/m. The model exhibits symmetry about the $x = 0$ plane. A rectangular coordinate system is established with original point O, located at the center of the lower end surface of the electromagnet. The center of mass of the ball lies on the $x = 0$ plane, with a position defined as $(0, y, z)$. Theoretically, the magnetic field generated by a hollow cylindrical solenoid is symmetric along the z-axis. The magnetic field of the magnetic ball at any position can be represented equivalently by that on the $x = 0$ plane. The angle between the N pole of the magnetic ball and the z-axis is defined as the magnetic pole orientation of the ball, denoted as θ. A negative value of θ indicates the counterclockwise direction.

$$\nabla\cdot\mathbf{B} = 0, \quad \nabla\times\mathbf{B} = \mu_0\mathbf{J}, \quad \nabla\times\mathbf{E} = -\frac{\partial\mathbf{B}}{\partial t}, \tag{5}$$

where ∇ is the gradient operator $\mathbf{B}$ is magnetic flux density, $\mathbf{E}$ is electric field intensity, and $\mathbf{J}$ is the current density.

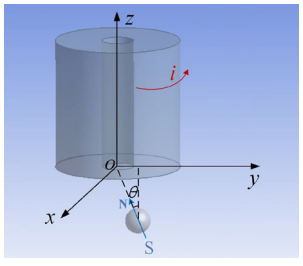

Fig. 5. Physical model of a magnetically levitated ball system

The model is calculated and simulated under various working conditions using a magnetostatic solver. The parameter values for electromagnetic field simulation are shown in Table 2. Each parameter is valued at uniform intervals within a specified range. The magnetic field generated by the hollow cylindrical electromagnet is centrally symmetrical. To reduce the computational load, only the position of the ball in the right half-plane of $x=0$ is considered. Therefore, the y-coordinate of the magnetic ball is set to a positive value. The north pole of the energized electromagnet faces in the $+z$ direction. According to the law of magnetic attraction, the magnetic ball's north pole will orient towards the electromagnet. Consequently, the range of magnetic pole orientation for the ball is set from –90° to 90°.

Table 2. Range of magnetic field simulation parameters

Parameters	Range	Parameters	Range
y	0 mm to 30 mm	Magnetic pole orientation	–90° to 90°
z	–45 mm to 0 mm	Drive current	0 A to 3 A

2.4 Influence of Driving Current and Position

The influence of the driving current of an electromagnet on the electromagnetic force of the ball is investigated. Two distinct positions of the ball, referred to as position 0 and position 1, are

selected for analysis. Position 0 is characterized by a position of [0 mm, 8 mm, -36 mm] and a magnetic pole orientation θ of 0°, while position 1 has a position of [0 mm, 15 mm, –26 mm] and θ of 0°. Fig. 6 illustrates the variation of the electromagnetic force and torque on the ball as the current gradually increases from 0 A to 3 A. It is observed that both the electromagnetic force and torque of the ball exhibit a linear relationship with the current. As the current increases, the electromagnetic force and torque also increase gradually, due to the closer proximity of position 1 to the electromagnet compared to position 0. Consequently, under the same current, the electromagnetic force and torque for position 1 are greater.

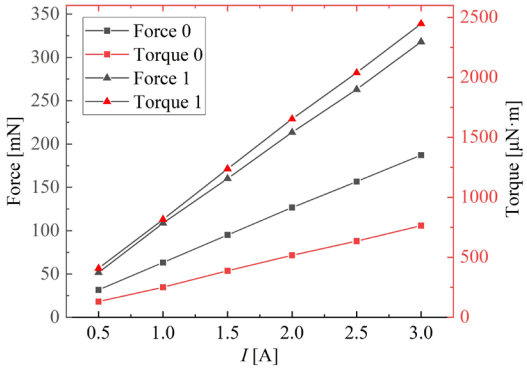

Fig. 6. Relationship between electromagnetic force, torque of the magnetic ball and the driving current of the electromagnet

As illustrated in Figs. 7a and c, the cloud diagram of the magnetic field distribution as the driving current of the magnetic ball at position 0 increases from 1 A to 2 A. The small black arrow indicates the direction of the magnetic pole of the magnetic ball. It is evident that the magnetic field surrounding the electromagnet and the magnetic ball exhibits a gradient distribution. As the current increases, the field strength near the electromagnet also increases.

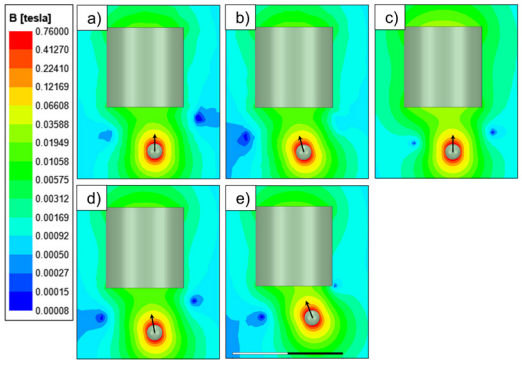

Fig. 7. Magnetic field cloud diagram of a magnetic ball and electromagnet in y-O-z plane where ball positions, magnetic pole orientation, and current are: a) [0 mm, 8 mm, -36 mm], θ = 0, I = 1 A; b) [0 mm, 8 mm, -36 mm], θ = -20, I = 1 A; c) [0 mm, 8 mm, -36 mm], θ = 0, I = 2 A; d) [0 mm, 8 mm, -36 mm], θ = -11, I = 1 A; and e) [0 mm, 15 mm, -26 mm], θ = 0, I = 1 A

The influence of the magnetic pole orientation of the magnetic ball on the electromagnetic effect is studied. The specific position of the ball is designated as [0 mm, 8 mm, –36 mm], with a driving current of 1 A applied to the electromagnet. The magnetic pole orientation of the magnetic ball is gradually varied from –90° to 90°. Fig. 8 illustrates the relationship between the electromagnetic force, torque, and the magnetic pole orientation exerted on the magnetic ball. As the magnetic pole orientation shifts in the positive direction, the magnetic ball undergoes clockwise rotation. Initially, the electromagnetic force of the magnetic ball increases, reaching a maximum value before subsequently decreasing. The torque of the magnetic ball is primarily directed along the x-axis, diminishing from the –x-axis direction to 0°, and then gradually increasing in the +x-axis direction. Clearly, the magnetic pole orientation of the ball significantly influences the electromagnetic force and torque. Fig. 7b depicts the contour map of the magnetic field distribution of the magnetic ball when the magnetic pole orientation θ is –20°. In comparison to θ of 0°, noticeable alterations are observed in the magnetic field distribution and the direction of the magnetic vector near the magnetic ball.

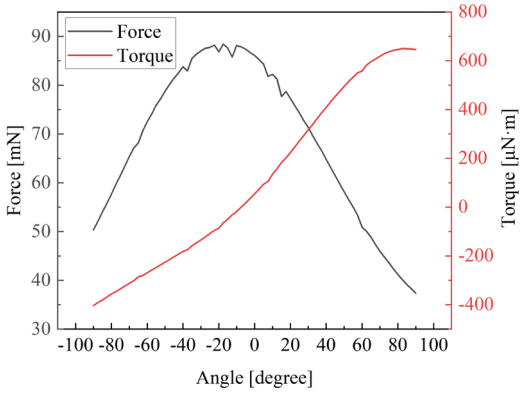

Fig. 8. Relationship between electromagnetic force and torque of the magnetic ball and magnetic pole orientation

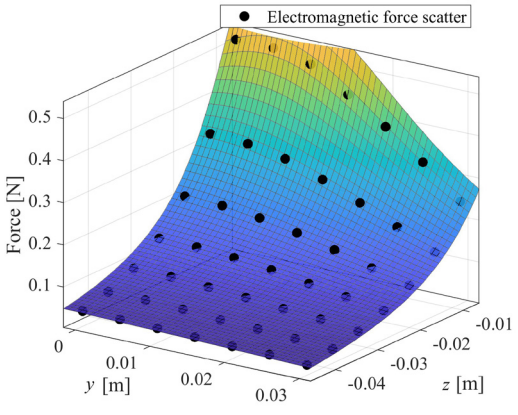

Fig. 9. Relationship between electromagnetic force and position of magnetic ball at different positions

The magnetic pole angle of the ball is calculated while the magnetic torque is zero. Fig 9 presents a scatter plot of the electromagnetic force on the magnetic ball at different positions, along with its fitted surface. Fig. 10 shows the calculated magnetic pole orientations at different positions when the electromagnet's driving current is 1 A and the torque of the ball is balanced. Fig. 7d shows the magnetic field distribution cloud diagram when the ball is located at the position [0 mm, 8 mm, –36 mm]. The calculated magnetic pole orientation is –11° as the ball's torque is balanced. Fig. 7e shows the magnetic field distribution cloud diagram when the ball is located at the position [0 mm, 15 mm, –26 mm]. The calculated magnetic pole orientation is –26° as the ball's torque is balanced. When fitting the electromagnetic force, the expression for the electromagnetic force in Eq. (1) becomes overly complex when expanded, so a simplified formula is typically used for approximation. According to literature [26], the electromagnetic force exerted on a permanent magnet

by an electromagnet is proportional to the current and inversely proportional to the square of the distance, and it can be expressed as

$$F_m = \frac{eI}{\left(a\delta^2 + b\delta + c\right)}, \tag{6}$$

where δ is the distance between the electromagnet and the permanent magnet. The distance between the electromagnet and the permanent magnet is related to both the y and z coordinates, and Eq. (1) can be rewritten as

$$F_m = \frac{eI}{\left(ay^2 + by + cz^2 + dyz + h\right)}, \tag{7}$$

where a, b, c, d, e, and h are constants. The values obtained from fitting results a = 2.25 × 10–5, b = –0.705, c = 2.086, d = –1.093, e = 3.06 × 10–4, and the goodness of fit is 0.996. The units of I, y and z are A, m and m within Eq. (7), respectively.

In Fig. 10, it can be seen that when the magnetic ball is subjected to the magnetic field of the electromagnet, the orientation of the magnetic poles is either zero or negative, tending toward the center of the electromagnet. When y = 0, meaning the ball is positioned along the axis of the electromagnet, the orientation of the magnetic poles aligns with the +z-axis direction. As the ball moves further away from the axis, the relative deviation angle of the magnetic pole orientation increases, resulting in a more rapid change in the magnetic pole orientation of the ball in the y-direction. As illustrated in Fig. 10, as the magnetic ball approaches the center of the lower end face of the electromagnet, the electromagnetic force intensifies. The rate of change of the electromagnetic force in the z-axis direction exceeds that in the y-axis direction. Consequently, the z-coordinate position of the magnetic ball significantly influences the electromagnetic force. Near the lower end face of the electromagnet, the field strength in the z-axis direction diminishes more rapidly than in the y-axis direction, resulting in a larger magnetic field gradient.

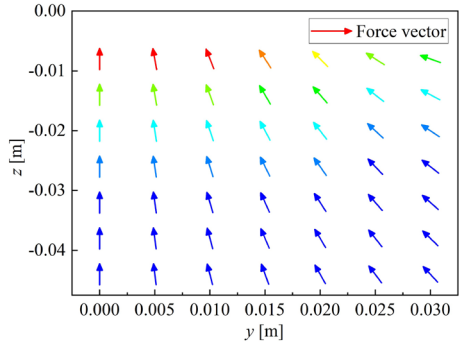

Fig. 10. Relationship between magnetic pole orientation and position of magnetic ball

3 RESULTS

3.1 Blood Flow Field Simulation Method

Simulations were conducted using Fluent software to analyze the blood flow environment surrounding the magnetic ball. Fig. 11 illustrates the fluid simulation model of the magnetic ball within a straight blood vessel. The blood fluid domain was cylindrical, with a diameter of 22 mm and a length of 100 mm. Blood flowed horizontally, and the magnetic ball was fully contained within the vessel. Point P represented the center of the magnetic ball, and the origin of the coordinate system is located at the center of the fluid domain's axis. The velocity inlet was set at the left end face of the fluid domain, while the right end face was designated as the zero-pressure outlet. A standard k–ε epsilon model is used for turbulent modeling due to accuracy and stability. To simplify the model, blood was treated as a Newtonian fluid with a density of 1060 kg/m3 and a viscosity of 3.5×10–3 Pa·s due to the similarity between the blood and Newtonian fluid. The continuity equation and the Navier-Stokes equations were employed to describe characteristic variations of fluid, and the control equations were discretized and solved iteratively using the finite volume method. The coupling relationship between velocity and pressure was managed using the SIMPLE algorithm.

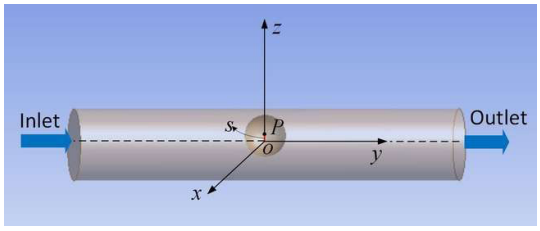

Fig. 11. Physical model of intravascular flow

The position of the ball in the vertical direction is considered an important influencing variable, which is represented by s relative to the origin O, as shown in Fig. 11. Positive values indicate that the position is located in the positive half of the z-axis. After parameterizing the vertical position s of the ball and the blood flow velocity v, finite element simulation calculations are conducted separately. Table 3 shows the range and interval of parameterization for both the vertical position of the magnetic ball and the blood flow velocity.

Table 3. The parameter range of blood flow field simulation

Parameter	Value	Parameter	Value
s	–4 mm to 4 mm	v	0.08 m/s to 0.24 m/s

3.2 The Effect of the Ball's Position and Blood Flow Velocity on Fluid Force

In the coordinate system depicted in Fig. 11, the position of the magnetic ball within the blood vessel can be characterized by its distance from the center of the vessel. Since the z-axis in the magnetic levitation ball system represents the direction of the magnetic force of the ball, the position change of the ball in the z-direction matters. Simulation results indicate that the maximum magnitude of the fluid force on the magnetic ball in the x-direction is on the order of 10–5 N, which can be considered negligible.

The fluid forces acting on the magnetic ball in the y- and z-directions are examined. The y-direction represents the direction of blood flow, while the z-direction indicates the vertical orientation. Fig. 12 illustrates the relationship between the force exerted on the magnetic ball in the direction of blood flow and the blood flow velocity. It is evident that when the vertical position of the ball remains constant, the fluid resistance acting on the ball in the direction of blood flow gradually increases as the blood flow velocity rises. When the blood flow velocity exceeds 0.16 m/s, a linear relationship emerges between fluid resistance and blood flow velocity. The fluid resistance curves for the vertical positions of the ball at 2 mm and –2 mm nearly overlap, as do the curves for the vertical positions of the ball at 4 mm and –4 mm. This indicates that the fluid resistance on the ball in the direction of blood flow depends on the distance s between the ball and the axis of the blood vessel. Fig. 13 presents the relationship between the force on the ball in the direction of blood flow and the vertical position. It can be observed that when the blood

flow velocity remains constant, the fluid resistance on the ball in the direction of blood flow increases as the s increases. At a high blood flow velocity of 0.24 m/s, the fluid resistance increases more rapidly as the s increases, with a maximum value of 7.7 mN.

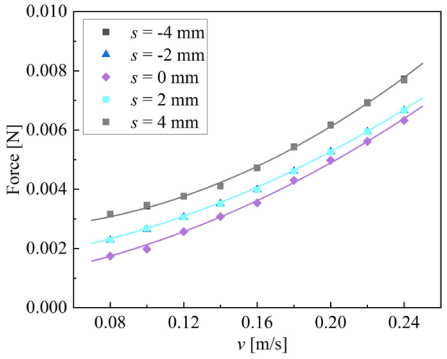

Fig. 12. The relationship between the fluid force exerted on the ball in the blood flow direction and the blood flow velocity

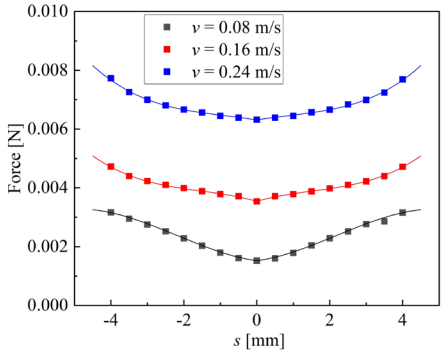

Fig. 13. The relationship between the fluid force on the ball in the direction of blood flow and its vertical position

The curves presented in Figs. 12 and 13 are the fitted curves for the fluid force scatter data. From Eqs. (3) and (4), it can be seen that the flow velocity affects the fluid force through both proportional and quadratic relationships. Then an empirical cubic equation is added to describe the influence of the vertical position s, so the expression for the fluid force is as follows:

$$F_d = \left(\mathrm{a}'v^2 + \mathrm{b}'v + \mathrm{c}'\right)\left(\mathrm{d}'s^3 + \mathrm{e}'s^2 + \mathrm{g}'s + \mathrm{h}'\right), \tag{8}$$

where the constants a', b', c', d', e', g', h' have values of: 10.03, 0.38, 0.208, 0.456, 10.07, 0.456, 0.0068, after fitting calculations with a goodness of 0.983. The units of v and s are m/s and mm within Eq. (8), respectively.

Fig. 14 depicts the relationship between the fluid force on the ball in the vertical direction and the vertical position. When the vertical position of the ball is at 0 mm and ±2 mm, the vertical force on the ball approaches zero. However, when the vertical position of the ball is at ±4 mm, the vertical force on the ball gradually increases as the blood flow velocity rises.

In Fig. 14, it is evident that as the distance of the ball's deviation from the axis of the blood vessel increases, the vertical fluid force also rises. When both the blood flow velocity and the vertical position of the ball are minimal, the vertical fluid force is correspondingly low, approaching zero. Conversely, when the blood flow velocity and vertical position are substantial, the vertical fluid force exerted on the ball becomes significant. When the ball deviates from the axis of the blood vessel by 4 mm, the vertical fluid force experiences a sudden increase, with the maximum force of 1.5 mN.

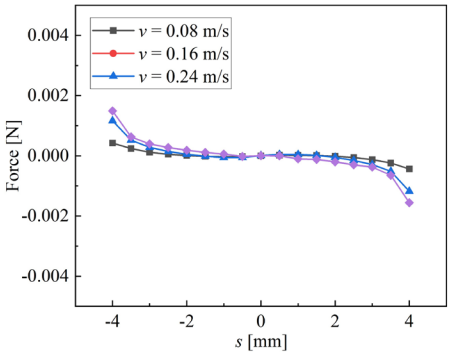

Fig. 14. The relationship between the fluid force exerted on the ball in the vertical direction and its vertical position

After calculations, the magnitude of the torque experienced by the magnetic ball in the blood vessel in the y-direction and z-direction is 10^{-8} N·m, and the magnitude of the torque experienced by the ball in the z-direction is 10^{-7} N·m. Therefore, they are not taken into account.

Fig. 15 illustrates the pressure cloud diagram of blood flow at varying velocities, with the ball positioned 2 mm above the axis of the blood vessel. Fig. 16 presents the shear stress distribution on the surface of the ball under the corresponding conditions. Fig. 17 depicts the corresponding blood velocity vector diagram. In Fig. 15, it is evident that when the ball is positioned above the axis of the blood vessel, a significant pressure differential exists between the fluid regions in front of and behind the ball. The pressure behind the ball is higher than that in front, resulting in a forward pressure gradient resistance. Furthermore, a notable pressure difference is observed on the upper and lower surfaces of the ball, causing the direction of the pressure gradient resistance to tilt slightly downward and exert a vertical downward force. Fig. 16 reveals that the shear stress on the rear surface of the ball exceeds that on the front surface, creating a forward viscous resistance. Consequently, the fluid resistance in the direction of blood flow comprises both pressure difference resistance and viscous resistance. In the vertical direction, the magnetic ball's resistance is primarily attributed to pressure difference resistance.

Fig. 17 shows that the inlet and outlet velocities of the blood vessel are essentially equivalent. However, in the region between the ball and the blood vessel wall, the flow velocities on either side differ. As the velocity of blood flow increases, both the pressure and flow velocity of the incoming fluid rise. Consequently, the differential pressure resistance and viscous resistance acting on the ball also increase significantly. Therefore, the fluid forces exerted by the ball in both the vertical and blood flow directions intensify as the blood inlet velocity increases.

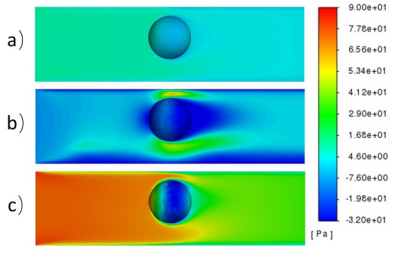

Fig. 15. Dynamic pressure cloud diagram in y-O-z plane of blood vessel under different blood flow velocity; a) v = 0.08 m/s, b) v = 0.16 m/s, and c) v = 0.24 m/s

Fig. 18 shows the pressure cloud diagram of the blood at various vertical positions of the ball when the blood flow velocity is 0.16 m/s. Fig. 19 shows the corresponding shear stress cloud diagram on the surface of the ball. Fig. 20 depicts the associated velocity vector

diagram of the blood. When the ball is positioned along the axis of the blood vessel, the flow field surrounding the ball is symmetric along this axis. The shear stress and pressure on the surface of the ball are greater on one side in the direction of the incoming flow, and they are symmetrically distributed on the upper and lower sides, as shown in Figs. 18c and 19c. The direction of the viscous drag and pressure difference resistance aligns with the direction of blood flow, resulting in a net vertical force of zero on the ball. However, when the ball deviates from the axis of the blood vessel, the shape of the blood flow around the ball becomes asymmetrical. Consequently, the blood flow velocity and pressure increase on the side where the space is narrower, altering the pressure distribution on the surface of the ball.

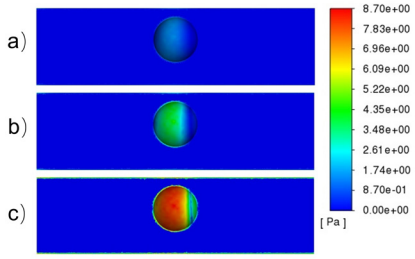

Fig. 16. Shear stress cloud diagram on the surface of the ball at different blood flow velocity

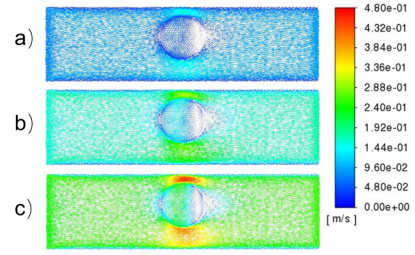

Fig. 17. Velocity vector cloud diagram at different blood flow velocity in the y-O-z plane of the vessel; a) v = 0.08 m/s, b) v = 0.16 m/s, and c) v = 0.24 m/s

When the vertical position of the ball is above the axis of the blood vessel, the pressure on the side of the ball adjacent to the vessel wall increases. The direction of the pressure difference resistance points toward the lower right, as indicated in Fig. 18d, while the direction of the viscous resistance acting on the ball points to the right, as shown in Fig. 19d. Consequently, the fluid force acting on the ball is directed toward the lower right, with the vertical component of the fluid force directed downward, resulting in a negative value for the force. Conversely, when the ball is positioned below the axis of the blood vessel, the vertical component of the fluid force is directed upward, yielding a positive value.

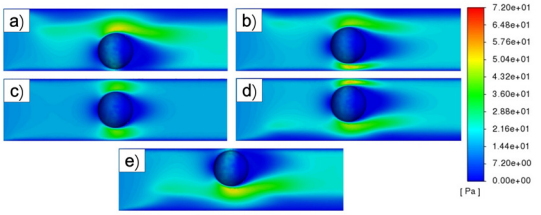

Fig. 18. Dynamic pressure cloud diagram in y-O-z plane of blood vessel; a) s = –4 mm, b) s = –2 mm, c) s = 0 mm, d) s = 2 mm, and e) s = 4 mm

As the vertical position of the ball increases relative to the axis of the blood vessel, the flow velocity near the upper surface of the ball also increases, resulting in a corresponding increase of shear force on that surface. Consequently, the vertical downward component of shear stress increases. Furthermore, as the distance between the ball and the axis of the blood vessel increases, both the vertical and horizontal components of the pressure difference increase. When the distance between the ball and the axis of the blood vessel is small, the shear stress distribution on the surface of the ball remains relatively constant. As shown in Figs. 19a and b, when the ball is close to the vessel wall, the shear stress on the side adjacent to the wall significantly increases. This leads to an increase in the vertical component of viscous resistance acting on the ball. Therefore, as the position s increases, the horizontal fluid resistance of the ball markedly intensifies. The vertical fluid force exhibits a noticeable increase only as the position s has a substantial value.

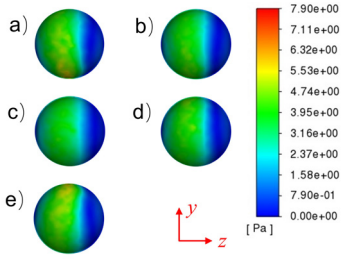

Fig. 19. Shear stress cloud diagram on the surface of the ball; a) s = –4 mm, b) s = –2 mm, c) s = 0 mm, d) s = 2 mm, and e) s = 4 mm

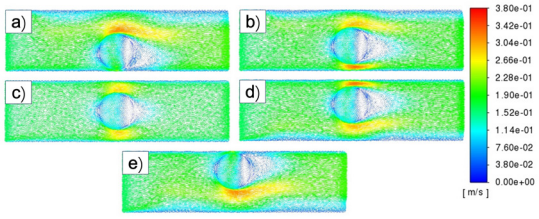

Fig. 20. Velocity vector cloud diagram of y-O-z plane of blood vessel and surface of ball; a) s = –4 mm, b) s = –2 mm, c) s = 0 mm, d) s = 2 mm, and e) s = 4 mm

Based on the fluid simulation results of the ball within the blood vessels, it can be observed that the ball experiences fluid forces in both the direction of blood flow and the vertical direction within the blood vessels. The fluid forces in the vertical direction are relatively smaller. The blood flow velocity and the position of the ball affect the distribution of the pressure field and velocity field of the blood, thereby influencing the magnitude and direction of the pressure difference resistance and viscous resistance of the ball. Both the blood flow velocity and the distance of the ball from the axis of the blood vessel contribute to an increase in the fluid forces acting on the ball.

3.3 Electromagnetic Field and Blood Flow Field Co-Simulation

Under the influence of appropriate electromagnetic field and blood flow field, magnetic balls can achieve force balance and remain suspended within blood vessels. The ANSYS Workbench platform integrates the Maxwell solver and the Fluent solver to simultaneously simulate both the electromagnetic field and the flow field. The resulting data is then transferred to the optimization module to calculate the steady-state physical parameters necessary for the levitation of the magnetic ball.

First, a three-dimensional model is created in Workbench based on the actual physical dimensions, as shown in Fig. 21. The origin of the coordinate system is positioned at the center of the lower surface of the electromagnet, with the direction of blood flow oriented along the $+y$ axis. The electromagnet is situated directly above the blood vessel, exerting an attractive force on the magnetic ball. The distance

between the bottom surface of the electromagnet and the axis of the fluid domain is 30 mm. The entire physical model is symmetric about the $x = 0$ plane. Theoretically, when the system reaches a steady state, the stable position of the ball will be located in the $x = 0$ plane. The position of the ball varies within the $x = 0$ plane and is denoted as $p_n(0, y_e, z_e)$. The magnetic pole direction of the ball θ, the driving current of the electromagnet I, and the blood flow velocity v are considered as the parameters to be optimized. The range of parameter optimization is equivalent to that specified Table 2 and Table 3. The total force and moment experienced by the ball in force equilibrium are zero, as shown in Eqs. (9) and (10). This condition is selected as the optimization objective, with a tolerance of 0.1 %,

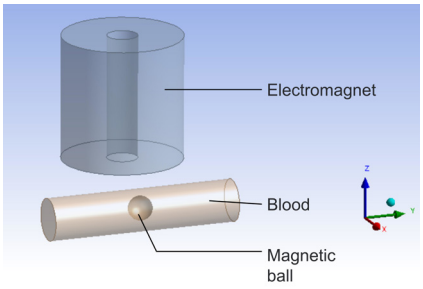

Fig. 21. Physical model of the co-simulation

$$F_e = 0 \Leftrightarrow \begin{cases} F_{mx} - F_{dx} = 0 \\ F_{my} - F_{dy} = 0, \\ F_{mz} - F_{dz} = 0 \end{cases} \tag{9}$$

$$T_e = 0 \Leftrightarrow \begin{cases} T_{mx} - T_{dx} = 0 \\ T_{my} - T_{dy} = 0, \\ T_{mz} - T_{dz} = 0 \end{cases} \tag{10}$$

where F_e is the resultant force on the ball, and F_{mx}, F_{my}, and F_{mz} are the components of the electromagnetic force in the *x, y,* and *z* directions, respectively. F_{dx}, F_{dy}, and F_{dz} are the fluid forces in the *x, y,* and *z* directions, respectively. T_e is the torque on the ball, and T_{mx}, T_{my}, and T_{my} are the components of the electromagnetic torque in the *x, y,* and *z* directions, respectively. T_{dx}, T_{dy}, and T_{dz} are the torque caused by fluid in the *x, y,* and *z* directions, respectively.

Multi-objective optimization is commonly used to design the parameters of mechanical structures [27]. In this study, the multi-objective genetic algorithm (MOGA) is employed to optimize the parameters of both the magnetic field and the flow field. Fig. 22 shows the flowchart of the MOGA optimization process. Initially, the variables are parameterized to generate the initial samples. Subsequently, the Maxwell and Fluent solvers are used to calculate the electromagnetic and fluid forces, which are then combined to determine the total forces and moments acting on the ball. The MOGA generates a new set of samples through hybridization and mutation to repeat the calculations. If the results meet the optimization objectives within the specified Pareto error, the calculation concludes, and the results are output. Otherwise, the generation of new samples continues for iterative calculations. The initial number of samples for optimization is set to 42, with 42 samples generated in each subsequent iteration.

The MOGA optimization process generated 287 design points and identified the three best candidate solutions. The parameters of these candidate solutions are presented in Table 4, with each result corresponding to a specific set of physical field parameters when the magnetic ball is in a state of steady equilibrium within the blood.

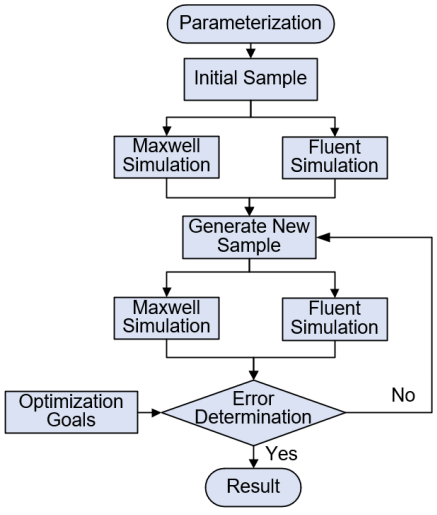

Fig. 22. Flow chart of MOGA optimization

Table 4. Results of MOGA optimization

Condition	Drive current [A]	Blood flow velocity [m/s]	Ball's position [mm]	N pole orientation of the ball [°]
A	0.5	0.14	(0, 1.53, –26.2)	7.7
B	0.75	0.09	(0, 0.50, –28.2)	2.6
C	1.2	0.18	(0, 2.37, –32.5)	5.1

4 DISCUSSION

An experiment was conducted to investigate the behavior of a magnetic ball's stable suspension within a fluid tube, and to validate the results of previous multi-objective optimization. As shown in Fig. 23, a mixture of water and glycerol (in a 2.3:1 mass ratio) was used as a substitute for blood, as it possesses similar density and viscosity characteristics. The fluid is propelled through the pipeline by a pump, with an adjustable flow rate. The magnetic levitation ball system consists of an electromagnet, a drive circuit, a controller, and a power supply. The magnetic ball is suspended within a fluid tube located beneath the electromagnet.

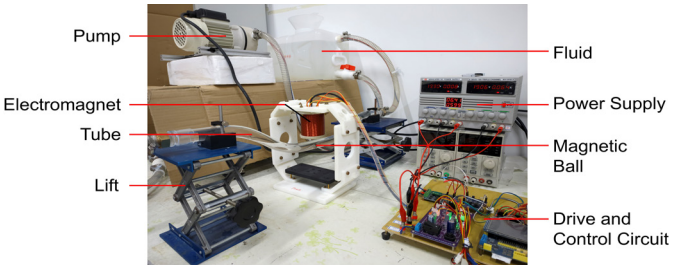

Fig. 23. Magnetic levitation experimental device

Fig. 24 presents photos of a magnetic ball in steady-state suspension within a fluid pipe at various flow velocities and different vertical positions. The green line indicates the central axis of the driver and the tube as a reference, while the red elliptical line outlines the ball. The '+' symbol marks the center of the ball. The sides of the ball appear elliptical due to refraction of light, which has been acounted. It can be seen that under the influence of the fluid, the suspension position of the ball deviates differently from the axis of the electromagnet. The driving current of the driver is adjusted to change the vertical levitation position of the ball within the fluid tube.

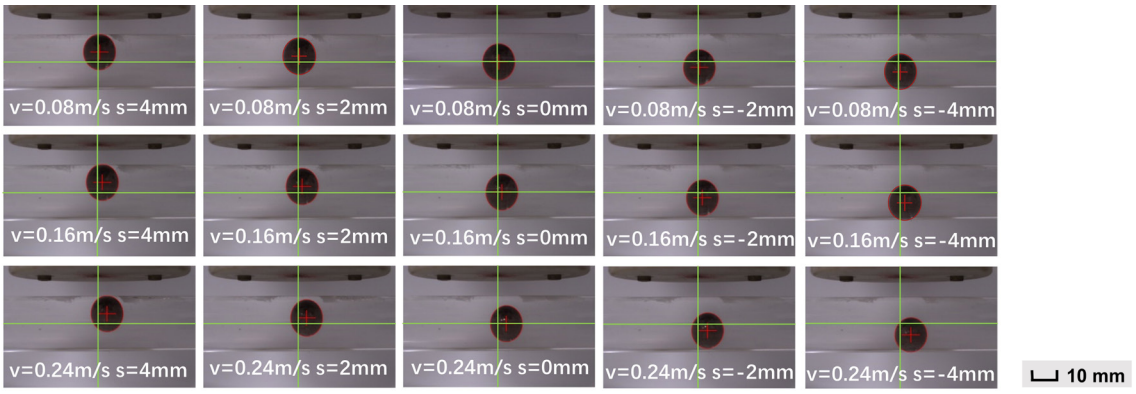

Fig. 24. Photos of a steady suspended ball in different conditions

Fig. 25 illustrates the relationship between the driving current of an electromagnet and the vertical position of a magnetic ball at various flow rates. This relationship is approximately linear; however, a sudden change of the driving current occurs when the ball reaches the extreme position near the tube wall (s = ±4 mm). As the driving current increases, the suspended position of the ball descends. According to the formula for the magnetic force of an electromagnet, the further the ball is from the electromagnet, the weaker the electromagnetic field becomes, necessitating a greater driving current to maintain force equilibrium. Additionally, at the same vertical position, the flow rate of the liquid has a minimal influence on the driving current required for suspension.

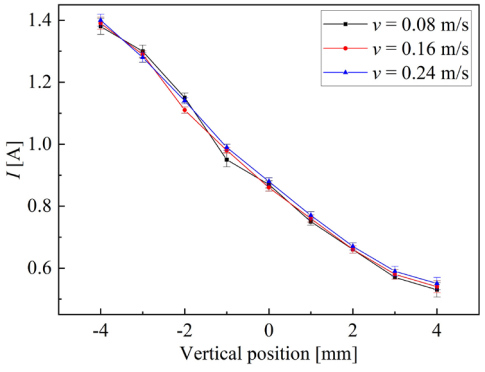

Fig. 25. Relationship between the driving current of an electromagnet and the vertical position of the magnetic ball

Fig. 26 illustrates the steady-state suspension trajectories of the magnetic ball at three different flow velocities. As the flow velocity increases, the horizontal displacement of the ball also increases. It is evident that at higher fluid velocities, the horizontal displacement of the ball increases while the vertical position of the suspended ball decreases.

The experimental results indicate that both the driving current of the electromagnet and the fluid flow velocity influence the steady suspension position of the magnetic ball within the tube. The driving current is the primary parameter affecting the vertical position of the ball, while the fluid flow velocity predominantly influences the horizontal position. Fig. 27 illustrates the force analysis of the ball at four positions, where the ball achieves force equilibrium during steady suspension. The electromagnetic force $\mathbf{F_m}$ acting on the ball always points toward the central region of the electromagnet along the magnetic field lines, while the fluid resistance $\mathbf{F_d}$ primarily acts in the horizontal direction. The gravity $\mathbf{G}$ and buoyancy $\mathbf{F_u}$ in the horizontal direction remain constant. When the magnetic ball encounters horizontal fluid resistance, it must deviate from the z-axis to generate a horizontal component of electromagnetic force that counteracts the fluid resistance and maintains force equilibrium. Initially, the ball can be stably suspended at position p_1, where the resultant force is zero. An increase in fluid flow velocity results in heightened viscous and pressure drag acting on the ball, leading to an increase of $\mathbf{F_d}$. To maintain force equilibrium, $\mathbf{F_m}$ must increase and shift direction, which can be proved by the increase in current with the increase in flow rate, as shown in Fig. 25. Consequently, the ball shifts position from p_1 to p_2 or p_4, with a significant increase in horizontal offset.

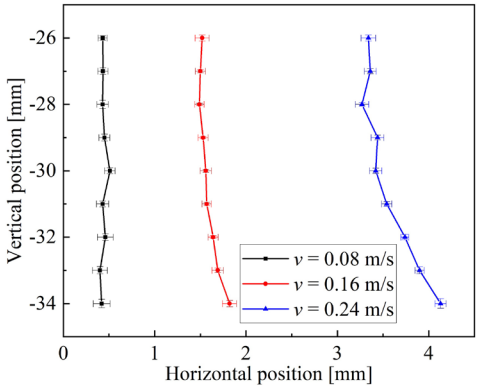

Fig. 26. The leviation trajectory of the magnetic ball within the fluid tube

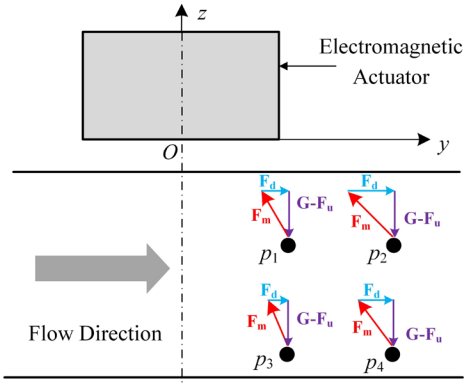

Fig. 27. Analysis of forces acting on a magnetic ball at various positions within a fluid tube

As seen in Fig. 8 and Fig. 12, the direction of the electromagnetic force rotates anticlockwise when the magnetic ball moves away from the electromagnet. The angle of deflection increases with an increase in horizontal position and decreases with a decrease in vertical

position. Additionally, the ball's fluid force $\mathbf{F_d}$ is greater when it is positioned further from the axis of the tube. As the vertical position s of the ball decreases, the magnetic ball must be deflected to the right and alter the direction of $\mathbf{F_m}$ for counteracting the increase in $\mathbf{F_d}$. The direction of the electromagnetic force then shifts to that shown at position p_4 while the ball reaches a new force equilibrium. Therefore, the horizontal offset distance increases as the position of the ball decreases, changing from p_1 to p_4.

The parameters of the three optimized results from Table 4 were applied in practical experiments to determine the actual suspended position of the ball. The comparison between the experimental results and the optimization results is presented in Table 5. In this study, the suspension of the magnetic ball occurs within a limited area, and the accuracy of the optimization results requires evaluation. To avoid the influence of the selection of the origin of the reference coordinate system on the error analysis, fiducial error [28] is used to evaluate the error between the simulation results and the experimental results, calculated as follows:

$$e = \frac{\Delta l}{\Delta d} \cdot 100\ \%, \tag{11}$$

where Δl represents the difference between the simulated value and the measured value, and Δd is the range of the magnetic ball's position. The range for the horizontal position is set to 30 mm, and the range for the vertical position is set to 45 mm.

The simulation error in condition C is greater than in the other conditions. This discrepancy is likely due to the large distance between the ball and the electromagnetic coil, resulting in a measurement accuracy of the linear Hall sensor. Overall, when the magnetically driven ball is stably suspended within the tube, the error between its position and the simulation results remains within 2 %, indicating that the simulation model is acceptable.

Table 5. Comparison between the experimental results and the optimization results

Condition	Simulation results [mm]	Experimental results [mm]	Y error [%]	Z error [%]
A	(0, 1.53, 3.8)	(0, 1.43, 3.1)	0.3	1.56
B	(0, 0.50, 1.8)	(0, 0.75, 1.2)	0.83	1.33
C	(0, 2.37, –2.5)	(0, 3.22, –1.7)	1.83	1.78

5 CONCLUSION

This study presents the design of a magnetic levitation ball system within a fluid tube, in which a magnetic ball is driven by an external magnetic field generated by an electromagnet. This system serves as a prototype for micro-mechanical diagnosis and therapy within the human circulatory system. Finite element numerical simulations of the electromagnetic field and blood flow are conducted to investigate the effects of blood flow velocity and the ball's position on fluid resistance, as well as the influence of position and angle on the magnetic force. Furthermore, a co-simulation of the flow field and magnetic field surrounding the magnetic ball is executed on the ANSYS Workbench platform. Based on the MOGA optimization, the physical field parameters for the steady-state levitation of the magnetic ball are calculated and verified through experiments. A comparison between the simulation and experimental results is presented. Finally, the characteristics of the steady-state suspended position of the magnetic ball are analyzed. The following conclusions can be drawn from this study:

1. An increase in the driving current or a decrease in the distance from the electromagnet results in a greater electromagnetic force of the magnetic ball. The gradient of the electromagnetic force along the axial direction of the electromagnet is observed to be greater than that along the radial direction. When the magnetic ball reaches a state of torque equilibrium under the influence of the electromagnet, its magnetic poles deviate and align toward the electromagnet.
2. The forces acting on the ball within the blood vessel are attributed to viscous resistance and pressure difference resistance. An increase in blood flow velocity and the distance of the ball from the axis of the blood vessel contribute to a rise in fluid resistance. The force exerted on the ball in the direction perpendicular to the blood flow is relatively small, while the fluid resistance in the direction of blood flow is significant.
3. The driving current of the electromagnet is the primary factor influencing the vertical position of the magnetic levitation ball, while the liquid flow velocity predominantly affects its horizontal position. At high blood flow rates, the horizontal position of the magnetic sphere is more significantly influenced by the driving current. As the driving current increases, the suspension height of the magnetic ball decreases, leading to a greater horizontal displacement.
4. An effective simulation model of a magnetically driven ball in a blood environment, along with a method for multi-objective optimization of parameters, is developed to determine the steady-state levitation parameters of the ball.

References

[1] Cai, Z., Fu, Q., Zhang, S., Guo, S., Guo, J., Zhang, X., Fan, C. Characteristic analysis of a magnetically actuated capsule microrobot in medical applications. *IEEE T Instrum Meas* 71, 4001511 (2021) **DOI:10.1109/TIM.2021.3130299**

[2] Schmidt, C.K., Medina-Sánchez, M., Edmondson, R.J., Schmidt, O.G. Engineering microrobots for targeted cancer therapies from a medical perspective. *Nat Commun* 11, 5618 (2020) **DOI:10.1038/s41467-020-19322-7**

[3] Zhang, D., Gorochowski, T.E., Marucci, L., Lee, H.T., Gil, B., Li, B., et al. Advanced medical micro-robotics for early diagnosis and therapeutic interventions. *Front Robot AI* 9, 1086043 (2023) **DOI:10.3389/frobt.2022.1086043**

[4] Elnaggar, A., Kang, S., Tian, M., Han, B., Keshavarz, M. State of the art in actuation of micro/nanorobots for biomedical applications. *Small Sci* 4, 2300211 (2024) **DOI:10.1002/smsc.202300211**

[5] Li, D., Choi, H., Cho, S., Jeong, S., Jin, Z., Lee, C., Ko, S. Y. et al. A hybrid actuated microrobot using an electromagnetic field and flagellated bacteria for tumor-targeting therapy. *Biotechnol Bioeng* 112, 1623-1631 (2015) **DOI:10.1002/bit.25555**.

[6] Fu, Q., Guo, S., Guo, J. Conceptual design of a novel magnetically actuated hybrid microrobot. *IEEE International Conference on Mechatronics and Automation*, 1001-1005 (2017) **DOI:10.1109/ICMA.2017.8015953**

[7] Zheng, L., Chen, L., Huang, H., Li, X., Zhang, L. An overview of magnetic micro-robot systems for biomedical applications. *Microsyst Technol* 22, 2371-2387 (2016) **DOI:10.1007/s00542-016-2948-6**

[8] Liang, N., Guo, J., Guo, S., Wei, X. Performance evaluation of the wireless micro robot in the fluid. *IEEE International Conference on Mechatronics and Automation*, 958-963 (2015) **DOI:10.1109/ICMA.2015.7237615**

[9] Larbi, M., Guechi, E.H., Maidi, A., Belharet, K. Observer-based control of a microrobot navigating within a 3D blood vessel along a trajectory delivered by a joystick device. *Machines* 11, 738 (2023) **DOI:10.3390/machines11070738**

[10] Qin, Y., Cai, Z., Han, J. Design and control of a magnetically-actuated anti-interference microrobot for targeted therapeutic delivery. *IEEE Robot Autom Let* 8, 5672-5679 (2023) **DOI:10.1109/LRA.2023.3295648**

[11] Marino, H., Bergeles, C., Nelson, B.J. Robust electromagnetic control of microrobots under force and localization uncertainties. *IEEE T Autom Sci Eng* 11, 310-316 (2013) **DOI:10.1109/TASE.2013.2265135**

[12] Chi, M., Zhang, J., Liu, R., Wang, Y., Nie, G., Qian, X. Coupled steering control of a low torsional torque capsule robot in the intestine. *Mechatronics* 77, 102596 (2021) **DOI:10.1016/j.mechatronics.2021.102596**

[13] Li, D., Niu, F., Li, J., Li, X., Sun, D. Gradient-enhanced electromagnetic actuation system with a new core shape design for microrobot manipulation. *IEEE T Ind Electron* 67, 4700-4710 (2019) **DOI:10.1109/TIE.2019.2928283**

[14] Liu, G., Lu, Y., Xu, J., Cui, Z., Yang, H. Magnetic levitation actuation and motion control system with active levitation mode based on force imbalance. *Appl Sci* 13, 740 (2023) **DOI:10.3390/app13020740**

[15] Estevez, P., Mulder, A., Munning Schmidt, R.M. 6-DoF miniature maglev positioning stage for application in haptic micro-manipulation. *Mechatronics* 22, 1015-1022 (2012) **DOI:10.1016/j.mechatronics.2012.08.002**
[16] Dabbagh, S.R., Alseed, M.M., Saadat, M., Sitti, M., Tasoglu, S. Biomedical applications of magnetic levitation. *Adv NanoBiomed R*, 2 2100103 (2022) **DOI:10.1002/anbr.202100103**
[17] Choi, K., Jang, G., Jeon, S., Nam, J. Capsule-type magnetic microrobot actuated by an external magnetic field for selective drug delivery in human blood vessels. *IEEE T Magn* 50, 1-4 (2014) **DOI:10.1109/TMAG.2014.2325055**
[18] Cha, K., Jeong, S., Choi, J., Qin, L., Li, J., Park, J. et al. Electromagnetic actuation methods for intravascular locomotive microrobot. *Annual International Conference of the IEEE Engineering in Medicine and Biology*, 1962-1965 (2010) **DOI:10.1109/IEMBS.2010.5627599**
[19] Qu, C., Pei, Y.-C., Xin, Q.-Y., Li, Z.-X., Xu, L. A reciprocating permanent magnetic actuator for driving magnetic micro robots in fluids. *P I Mech Eng C-J Mec* 235, 6451-6462 (2021) **DOI:10.1177/09544062211014547**
[20] Derbal, D., Bouzit, M., Mokhefi, A., Bouzit, F. Effect of the curvature angle in a conduit with an adiabatic cylinder over a backward facing step on the magnetohydrodynamic behaviour in the presence of a nanofluid. *Stroj Vestn-J Mech E* 69, 135-154 (2023) **DOI:10.5545/sv-jme.2022.239**
[21] Gkountas, A.A., Polychronopoulos, N.D., Sofiadis, G.N., Karvelas, E.G., Spyrou, L.A., Sarris, I.E. (2021). Simulation of magnetic nanoparticles crossing through a simplified blood-brain barrier model for Glioblastoma multiforme treatment. *Comput Meth Prog Bio* 212, 106477 **DOI:10.1016/j.cmpb.2021.106477**
[22] Ali, F., Sheikh, N.A., Khan, I., Saqib, M. (2017). Magnetic field effect on blood flow of Casson fluid in axisymmetric cylindrical tube: A fractional model. *J Magn Magn Mater* 423, 327-336 **DOI:10.1016/j.jmmm.2016.09.125**
[23] Belharet, K., Folio, D., Ferreira, A. Control of a magnetic microrobot navigating in microfluidic arterial bifurcations through pulsatile and viscous flow. *Proceedings of the 2012 IEEE/RSJ International Conference on Intelligent Robots and Systems*, 2559-2564 (2012) **DOI:10.1109/IROS.2012.6386030**
[24] Yesin, K.B., Vollmers, K., Nelson, B.J. Modeling and control of untethered biomicrorobots in a fluidic environment using electromagnetic fields. *Int J Robot Res* 25, 527-536 (2006) **DOI:10.1177/0278364906065389**
[25] Tillack, M.S., Morley, N.B. *Magnetohydrodynamics, Standard Handbook for Electrical Engineers*, McGraw Hill (1988) New York
[26] Choi, J.S., Baek, Y.S. A single dof magnetic levitation system using time delay control and reduced-order observer. *KSME Int J* 16, 1643-1651 (2002) **DOI:10.1007/BF03021666**
[27] Li, L., Wang, S. Experimental study and numerical analysis on windage power loss characteristics of aviation spiral bevel gear with oil injection lubrication. *Strojn Vestn-J Mech E* 69, 235-247, (2023) **DOI:10.5545/sv-jme.2023.558**
[28] Zhao, J., Cui, C., Zhang, P., Wang, K., Zhao, M. Parameter sensitivity analysis of the seismic response of a piled wharf structure. *Buildings*, 13349 (2023) **DOI:10.3390/buildings13020349**

Acknowledgements *This work was supported by the National Natural Science Foundation of China (No.51975293) and Aeronautical Science Foundation of China (No.2019ZD052010).*

Received 2024-07-01, revised 2024-12-04, 2025-02-25, accepted 2025-03-05 *as Original Scientific Paper.*

Data availability *The data that support the findings of this study are available from the corresponding author upon reasonable request.*

Author contribution *Zhanxiang Cui: conceptualization, methodology, formal analysis, and writing – original draft; Yonghua Lu: writing – review & editing, Zezheng Wang: data curation and visualization; Ziyuan Wang: data curation and visualization; Yun Zhu: validation.*

Supplementary Information *The supplementary information includes the simulation results of the magnetic vector distribution of the magnetic ball and electromagnet, the calculation method of turbulence intensity in fluid simulation, the relationship between the fluid force of the magnetic ball and the blood flow velocity in fluid simulation, and the sensitivity analysis of parameters in MOGA optimization.*

Numerična in eksperimentalna študija stabilne levitacije magnetne krogle gnane z zunanjimi elektromagneti v cevki s tekočino: Uporaba v mikronapravah v človeških krvnih žilah

Povzetek *Raziskave na področju uporabe mikrorobotov v medicini uvajajo inovativne metode za zdravljenje različnih bolezni. Cilj te študije je razširiti uporabo nadzorovanih mikromehanskih diagnostičnih in terapevtskih pristopov znotraj človeških krvnih žil z zasnovo sistema magnetne levitacije krogle v cevki okroglega prereza, napolnjeni s tekočino. Sistem omogoča stabilno lebdenje magnetne krogle vzdolž določene poti pod vplivom zunanjega magnetnega polja. S pomočjo programske opreme so bile po metodi končnih elementov izvedene simulacije elektromagnetnega polja, tokovnega polja in mehanskega stanja sistema. Študija podaja analizo vpliva položaja krogle, usmerjenosti magnetnih polov, električnega toka in hitrosti toka tekočine na sile, ki delujejo na magnetno kroglo. Hkratna simulacija toka in magnetnega polja je bila izvedena na platformi ANSYS Workbench, pri čemer je bila uporabljena metoda večobjektne optimizacije za določitev parametrov, ki omogočajo stabilno levitacijo. Eksperimentalna potrditev je pokazala stabilno lebdenje magnetne krogle v tekočinski cevki pod vplivom zunanjega magnetnega polja. Eksperimentalni rezultati so potrdilo povezave med električnim tokom, hitrostjo toka tekočine in stabilnim položajem krogle, kar potrjuje natančnost simulacijske metode in izvedljivost nadzora položaja objektov v cevkah s tekočino.*

Ključne besede *magnetna levitacija, krvna žila, stabilna levitacija, biomedicinske naprave, večobjektna optimizacija*